Hybrid-DFT Study on Electronic Structures of the Active Site of Sweet Potato Purple Acid Phosphatase: The Origin of Stronger Antiferromagnetic Couplings than Other Purple Acid Phos...

ARTICLE *in* THE JOURNAL OF PHYSICAL CHEMISTRY A · MAY 2009

Impact Factor: 2.69 · DOI: 10.1021/jp8090123 · Source: PubMed

Hybrid-DFT Study on Electronic Structures of the Active Site of Sweet Potato Purple Acid Phosphatase: The Origin of Stronger Antiferromagnetic Couplings than Other Purple Acid Phosphatases

Kenichi Koizumi,*[,†,‡] Kizashi Yamaguchi,[§] Haruki Nakamura,[‡] and Yu Takano[‡]

Japan Biological Information Research Center, Aomi, Koto-ku, Tokyo 135-0064, Japan, Institute for Protein Research, Osaka University, Suita, Osaka 565-0871, Japan, and Center for Quantum Science and Technology under Extreme Conditions, Osaka University, Toyonaka, Osaka 560-8531, Japan

Received: October 11, 2008; Revised Manuscript Received: March 10, 2009

The electronic structure and magnetic interactions of the active site of sweet potato purple acid phosphatase (PAP) were investigated by using UHF, pure DFT (UBLYP), and hybrid DFT methods (UB3LYP and UB2LYP). PAP catalyzes the hydrolysis of a phosphate ester under acidic conditions and contains a binuclear metal center. Sweet potato PAP provides stronger antiferromagnetic coupling than other PAPs. UB3LYP showed reasonably good agreement with the experimental magnetic coupling, indicating that this stronger antiferromagnetic coupling is caused by a μ-oxo bridge in the Fe(III)−Mn(II) binuclear metal center, which is the origin of the asymmetric spin delocalization. The type of bridging ligand is essential for the reaction mechanism, because the bridging ligand is suggested to function as a nucleophile in the reaction. Analyses of the natural orbital and spin density distributions implied the asymmetric spin delocalization on the bridging oxygen. The mechanism and the pathway of the antiferromagnetic coupling between Fe(III) and Mn(II) were discussed, using chemical indices introduced with the occupation numbers of singly occupied natural orbitals.

1. Introduction

Purple acid phosphatase (PAP) catalyzes the hydrolysis of a phosphate ester under acidic conditions (pH range from 4 to 7). The enzymes are distinguished from other acid phosphatases by their characteristic purple color at around 560 nm, due to the presence of a tyrosine residue ligated to the ferric ion. The reaction mechanism, however, remains unclear. The active site of PAP consists of a binuclear metal center. A mammalian PAP contains a Fe(III)−Fe(II) center in the active site.[1−3] A Fe(III)−Zn(II) binuclear active site is present in the PAP from red kidney bean.[4] Recently, Schenk et al. have reported that a sweet potato PAP,[5,6] which shows higher turnover values than other PAPs, has an active site composed of Fe(III) and Mn(II) ions. In the active site, Asp134, Tyr166, and His324 coordinate to the Fe(III) ion, and Asn200, His285, and His322 to the Mn(II) ion. Asp163 acts as a bridge between the Fe(III) and Mn(II) ions. The oxygen observed between the Fe(III) and Mn(II) ions is regarded as a μ-oxo or μ-hydroxo bridge (Figure 1).

By analogy to the reaction mechanism of urease, H_2O or OH^- coordinating to the binuclear metal center was proposed to act as a nucleophile in the hydrolysis by PAP.[7,8] However, a recent ENDOR study on mammalian PAP has suggested that neither a water molecule nor a hydroxo ligand is attached to the Fe(III) ion.[9] This indicates that a nucleophile should be a bridging ligand. The reaction mechanism based on the concept of a nucleophilic bridging ligand has been proposed for the sweet potato PAP.[5] Therefore, the character of the bridging ligand is essential for the reaction mechanism.

The magnetic coupling constant, J, was determined to be about -10 cm^{-1} for the reduced form of the mammalian PAP, in which the binuclear metal center is bridged by a μ-hydroxo group.[10−13] Sweet potato PAP shows stronger antiferromagnetic coupling: $J < -70$ cm^{-1}, even though the amino acid residues ligated to the transition metals of sweet potato PAP are the same as those of mammalian PAP.[6] This result suggests that the bridging ligand of sweet potato PAP might be a μ-oxo group.[6] One of our aims in this study is to theoretically determine the bridging ligand in the active site of sweet potato PAP.

Symmetry-adapted (SA) CASCI and CASSCF, followed by the second-order perturbation correction, are useful for the quantitative theoretical treatment of multinuclear transition metal complexes. Such computations are difficult to apply to large systems containing transition metals, such as the active site of sweet potato PAP. We have studied many transition metal complexes, and have demonstrated the effectiveness of the broken-symmetry (BS) approach for elucidating the magnetic couplings of binuclear transition metal systems.[14,15] The BS methods can be regarded as alternative and practical approaches for theoretical studies on transition metal complexes.

There have been many DFT studies of the electronic structures of the active sites of metalloproteins. Siegbahn et al. investigated the mechanism of the O−O bond cleavage of the oxygen molecule catalyzed by methane monooxygenase and ribonucleotide reductase.[16] Yoon and Solomon studied the magnetic properties of the active site of ascorbate oxidase.[17] Noodleman et al. studied the spin coupling of iron sulfur clusters.[18] We have performed DFT calculations on the active site of hemerythrin, and discussed the magnetic interactions between the two iron parts via a bridging ligand.[19,20] A natural orbital analysis clearly revealed that the antiferromagnetism of the two irons is caused by a superexchange interaction via the bridging ligand. These results indicate that DFT methods provide

* To whom correspondence should be addressed. Phone: +81-6-6879-4311. Fax: +81-6-6879-8636. E-mail: koizumi@protein.osaka-u.ac.jp.
† Japan Biological Information Research Center.
‡ Institute for Protein Research, Osaka University.
§ Center for Quantum Science and Technology under Extreme Conditions, Osaka University.

10.1021/jp8090123 CCC: $40.75
Published on Web 04/08/2009

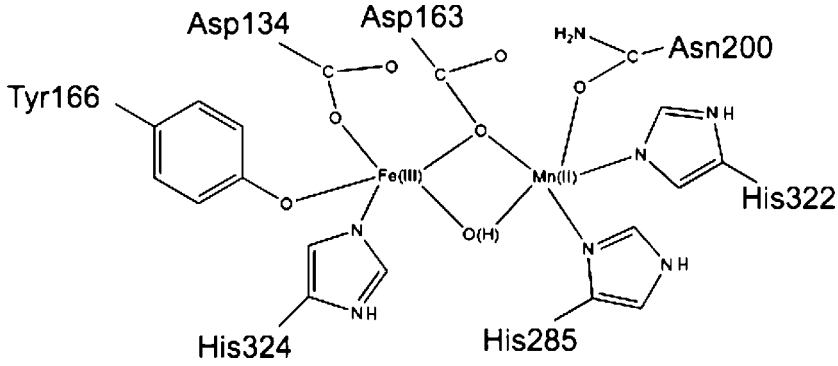

Figure 1. Schematic picture of the active site of sweet potato purple acid phosphatase.

reasonable electronic structures of the active sites of proteins including transition metals, when the exchange-correlation functionals are chosen appropriately.

In this study, we performed BS DFT calculations on the active site of sweet potato PAP, and investigated the origin of the characteristic magnetic interactions of the active site. UB3LYP reproduced the magnetic coupling constant determined by the magnetic susceptibility experiment. The calculated results strongly support the μ-oxo bridging ligand. We analyzed the spin and charge density distributions and the shapes of the natural orbitals. These results indicated that asymmetric spin delocalization on the Fe(III) ion and the bridging ligand, caused by the μ-oxo bridging ligand, is the main origin of the stronger antiferromagnetism, reflecting the asymmetrical nature of the bridging structure of the Fe(III)$-O^{2-}-$Mn(II) core.

2. Theoretical Background and Computational Details

2.1. Effective Exchange Integrals. We employed the Heisenberg Hamiltonian to describe the magnetic interaction between the magnetic sites.[21,22]

$$H = -2\sum_{ab} J_{ab}\mathbf{S}_a \cdot \mathbf{S}_b \tag{1}$$

The effective exchange integral, J_{ab}, can be estimated by using several computational methods, as follows

$$J_{ab} = \frac{^{LS}E_X - {}^{HS}E_X}{{}^{HS}\langle S^2\rangle_X - {}^{LS}\langle S^2\rangle_X} \tag{2}$$

where ${}^{Y}E_X$ and ${}^{Y}\langle S^2\rangle_X$ respectively denote the total energy and the total angular momentum of the spin states Y (Y = LS (lowest spin state) and HS (highest spin state)) by using the method X (X = UBLYP, UB3LYP, UB2LYP, and UHF).[23]

2.2. Computational Methods. The Kohn−Sham (KS) DFT is the practical method of computational chemistry.[24,25] The energy expression is given by

$$E = T_0[\{\psi_i\}] + V_{ne} + V_{Coulomb} + E_{XC}[\rho] \tag{3}$$

where T_0, $V_{ne,}$ and $V_{Coulomb}$ are the kinetic energy term of electrons, the energy term of nuclear−electron attraction, and the classical Coulomb energy term, respectively. E_{XC} is an exchange-correlation term. In a hybrid DFT such as B3LYP, E_{XC} can be described as follows

$$E_{XC} = C_1E_X^{HF} + C_2E_X^{Slater} + C_3E_X^{Becke88} + C_4E_C^{VWN} + C_5E_C^{LYP} \tag{4}$$

where the first and second terms on the right side of eq 4 indicate the Hartree−Fock exchange and the Slater exchange functionals, respectively. The third term is the Becke's exchange correction,[26] which includes the gradient of density, $\nabla\rho$. E_C^{VWN} and E_C^{LYP} are the Vosko, Wilk, and Nusair (VWN) correlation functional[27] and the correlation correction of Lee, Yang, and Parr (LYP),[28] respectively. C_i ($i = 1-5$) are the mixing parameters. They are (0.5, 0.5, 0.5, 1.0, and 1.0) for B2LYP (Becke's half and half LYP), (0.2, 0.8, 0.72, 1.0, and 0.81) for B3LYP, and (0, 1.0, 1.0, 1.0, and 1.0) for BLYP, respectively.[29]

2.3. Natural Orbitals. Singly occupied molecular orbitals (SOMOs) are nearly degenerate, because of the long Fe−Mn distance. Since it is difficult to analyze SOMOs, singly occupied natural orbitals (SONOs), which hold orbital symmetry, provide a clearer picture of magnetic interactions.[20,30] The NOs of the BS DFT solutions can be determined by diagonalization of their first order density matrices, as follows

$$\rho(\mathbf{r},\mathbf{r}') = \sum n_i\phi_i^*(\mathbf{r})\phi_i(\mathbf{r}') \tag{5}$$

where n_i is the occupation number of NO ϕ_i. The spin polarized MOs $\psi^+{}_i$ and $\psi^+{}_i$ for up and down spins can be connected with the in- and out-of-phase combinations of bonding and antibonding natural orbitals, as follows

$$\psi_i^+ = \phi_i\cos\theta_i \pm \phi_i^*\sin\theta_i \tag{6}$$

where θ_i is the mixing parameter. This is the relation between NO and MO. The orbital overlap T_i is defined as follows.

$$T_i = \langle\psi_i^+|\psi_i^-\rangle \tag{7}$$

By using the orbital overlap, T_i, the occupation numbers of the bonding and antibonding NOs can be expressed as follows

$$n_i = 1 + T_i, \quad n_i^* = 1 - T_i \tag{8}$$

where n_i and n_i^* correspond to the occupation numbers of bonding and antibonding NOs, respectively.

2.4. Chemical Indices. Chemical indices can be introduced by using the occupation numbers of the NOs, in order to investigate the character of the chemical bonding in the active site of sweet potato PAP. Since NOs can be defined in the SA picture, these indices can be regarded as the common concept in both the SA and BS pictures. We introduce the effective bond order b_i and the diradical character Y_i. The effective bond order is defined as follows.[31]

$$b_i = \frac{n_i - n_i^*}{2} \tag{9}$$

It indicates the strength of the covalent bond between the two magnetic sites. The diradical character[32] is defined as the weight of the doubly excited configuration.

$$Y_i = 1 - \frac{2T}{1+(T_i)^2} = \frac{(n_i)^2 - 4n_i + 4}{(n_i)^2 - 2n_i + 2} \quad (10)$$

It shows zero for a closed shell and one for a pure diradical state. These two indices can be used to indicate the instability of a chemical bond, although these parameters have different physical meanings.

2.5. Computational Details. UHF, pure DFT (UBLYP), and hybrid DFT (UB2LYP and UB3LYP)[29] calculations were performed on models of sweet potato PAP with Huzinaga's MIDI+p basis set (533(21)/53(21)/(41)) for transition metals,[33] the 6-31+G* basis set for the bridging ligand, 6-31G* for other heavy atoms,[34] and 6-31G for all H atoms.[35] All calculations were performed with the GAUSSIAN 03 program package.[36]

Models of the binuclear metal active sites bridged by a μ-hydroxo (**1**) or μ-oxo (**2**) group were prepared from the X-ray structure of sweet potato PAP[5] (PDB ID: 1XZW), determined at 2.5Å resolution at pH 4.9. As shown in Figure 2, the Asp residues (Asp 134, Asp163, and Asp200) were replaced with acetate ions, because of their pK_a value of 3.65. The His residues (His285, His322, and His324) were substituted with neutral methylimidazole, in spite of the pK_a value of 6.04, because these residues coordinate to the Fe and Mn ions of the active center. Tyr166 was truncated into a phenoxide ion. Since the reported X-ray structure of sweet potato PAP is the phosphate bound form, there is no structural information available about the bridging ligand of the binuclear active core in the resting state, in which the magnetic susceptibility was measured. We manually added the bridging ligand, OH or O, to the models and optimized the positions of the metal ions, the bridging ligand (μ-hydroxo or μ-oxo), and the hydrogen atoms of models **1** and **2** in the gas phase, at the UB3LYP level of theory. The total charges of models **1** and **2** are one and zero, respectively.

3. Results and Discussion

3.1. Effective Exchange Integrals, Optimized Structures, and Types of Bridging Ligand. We calculated the effective exchange integrals using eq 2 by UHF, UB2LYP, UB3LYP, and UBLYP. Table 1 summarizes the J_{ab} values for **1** and **2**. All of the calculations, except for UHF, yielded negative J_{ab} values for **1**, showing antiferromagnetic couplings between the Fe and Mn ions. All of the calculated J_{ab} values for **2** also indicated stronger antiferromagnetic couplings than those of **1**. The UHF method estimates smaller absolute values of the effective exchange integrals for **1** and **2**, whereas the UBLYP method provides larger values. Hybrid DFT methods, such as UB2LYP and UB3LYP, generate effective exchange integrals between those obtained by UHF and UBLYP.

As compared to the experimental result ($J_{ab} < -70$ cm^{-1}),[6] the absolute values of the calculated effective exchange integrals for **1** are smaller in all methods. This implies that a μ-hydroxo bridging ligand is inappropriate. The effective exchange integral for **2** estimated by UB3LYP is -69.22 cm^{-1}, which is close to the experimental J_{ab} value, suggesting that the UB3LYP method is the most reliable means of determining the electronic structures of **2**. Since the experimentally obtained absolute value of the effective exchange integral is larger than 70 cm^{-1}, we could employ UBLYP as an appropriate method for investigating the electronic structures of **1** and **2**. However, it is noted that UBLYP usually overestimates the antiferromagnetic couplings for transition metal complexes.[20,37]

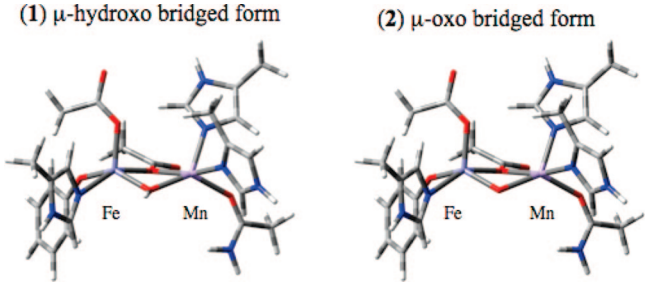

Figure 2. Models of the active sites of sweet potato purple acid phosphatase: μ-hydroxo-bridged form (**1**) and μ-oxo-bridged form (**2**).

TABLE 1: Effective Exchange Integrals (J_{ab}) for 1 and 2 Estimated by UBLYP, UB3LYP, UB2LYP, and UHF[a−c]

	J_{ab}	
method[d]	**1**	**2**
UBLYP	−28.50	−132.7
UB3LYP	−11.20	−69.22
UB2LYP	−2.971	−31.45
UHF	+0.684	−7.032

[a] J_{ab} values are shown in cm^{-1}. [b] J_{ab}(exp.) < −70 cm^{-1}. [c] The geometrical parameters of the metal ions, the bridging ligand (μ-hydroxo or μ-oxo), and the hydrogen atoms were optimized at the UB3LYP level of theory. [d] B2LYP means Becke's half and half LYP.

TABLE 2: Selected Geometrical Parameters for 1 and 2[a]

	1	**2**
Fe−Mn[b]	3.188	3.017
Fe−O[b]	1.953	1.778
Mn−O[b]	2.108	1.946
O−H[b]	0.968	
∠Mn−O−Fe[c]	103.4	108.1

[a] The positions of the metal ions, the bridging ligand (μ-hydroxo or μ-oxo), and the hydrogen atoms were optimized at the UB3LYP level of theory. [b] The distances are given in angstroms. [c] The angles are presented in degrees.

The partially optimized geometrical parameters are shown in Table 2. The optimized Fe−O bond distance is shorter than that of Mn−O. It reflects the asymmetrical Fe(III)−O^{2-}−Mn(II) or Fe(III)−OH^-−Mn(II) core. The bond lengths between the metal ion and the bridging oxygen in **1** are longer than those of **2**. This result indicated that the bonding nature of the Fe−O site is stronger in the case of model **2**. The Fe−O−Mn angle in **1** is smaller than that in **2**. In the previous study of the mangetic interactions of PPMn−OH−MnPP (PP = porphyrin), we concluded that the absolute value of effective exchange integral becomes larger as the Mn−O−Mn angle becomes close to 180°.[14] The larger angle of the Fe−O−Mn site contributes to the stronger antiferromagnetic interactions of **2**. According to ref 14 the difference of 5° causes at most 10 cm^{-1} difference in effective exchange integral in the case of PPMn−OH−MnPP.

UB3LYP geometry optimization always suffers from spin contamination error, due to the BS solution. Recently, Kitagawa et al. developed the approximately spin-projected geometry optimization method, which eliminated the spin contamination error.[38] For more detailed optimization, we need to employ such a method. However, the current UB3LYP calculation with the optimized structure reasonably reproduced the experimental J_{ab} values. Since it is well-known that the J_{ab} value is sensitive to the geometry of the transition metals and the bridging ligand, the spin contamination errors of the geometrical parameters thus obtained would be small.

TABLE 3: Mulliken Atomic Spin and Charge Densities for 1 and 2 in the LS State at the UB3LYP Level of Theory[a]

model		Fe	O	Mn	others
1	spin	4.04	0.09	−4.78	0.65
	charge	1.25	−0.68	1.15	−0.72
2	spin	4.02	0.40	−4.70	0.28
	charge	1.18	−1.03	1.07	−1.22

[a] The positions of the metal ions, the bridging ligand (μ-hydroxo or μ-oxo), and the hydrogen atoms were optimized at the UB3LYP level of theory.

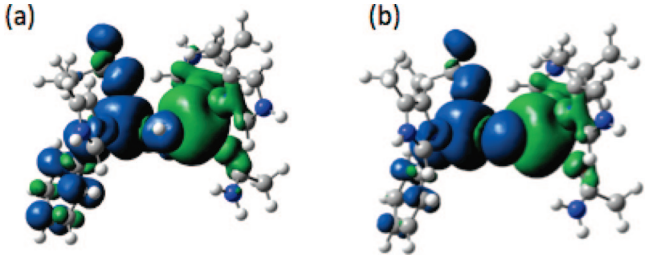

Figure 3. Spin density distributions of **1** (a) and **2** (b) in the LS states at the UB3LYP level of theory. Positive and negative spin densities are shown in blue and green, respectively.

3.2. Spin Densities and Charge Distributions. We investigated the Mulliken atomic spin and charge density populations of **1** and **2** to elucidate the characteristics of the charge transfers among the metal ions and the bridging ligand (μ-hydroxo or μ-oxo). As shown in Table 3, the spin density populations on the Fe(III) and Mn(II) ions decreased in **1** and **2**, although they are formally 5.0 in the high-spin state. The charge densities on the Fe(III) and Mn(II) ions in **1** and **2** also varied from the formal atomic charges. These results clearly indicate the strong donation from the amino acid residues and the ligand coordinating to the metal ions.

The Fe(III) ion tends to accept a β electron and exhibits a rather small spin density. Although the spin density on the O site of the μ-hydroxo ligand of **1** was about 0.0, positive spin density was observed on the μ-oxo ligand of **2**, indicating β electron delocalization (minority spin) from the μ-oxo ligand to the Fe(III) ion, leaving the majority of the α spin on μ-oxo. This is consistent with theoretical studies of oxy hemerythrin[20,39] and RNR.[15] Figure 3 clearly indicates that the charge transfer from the μ-oxo ligand mainly contributes to the β electron delocalization to the Fe(III) ion in **2**. Charge transfer from the coordinating amino acid residues to the Fe ion is responsible for the β electron delocalization in **1**, because the positive spin density on the residues of **1** is distributed more widely than that of **2**, as shown in Figure 3.

The spin density on the Mn(II) ion is reduced, as compared to the formal spin state of the Mn(II) ion, which is 5.0, implying the α spin delocalization to Mn(II) due to the charge transfer from the bridging ligand and the surrounding amino acid residues. These charge transfers to the metal ions are responsible for the superexchange interaction between the Fe and Mn ions via the bridging ligand. However, the charge transfer was larger on the Fe(III) ion in all methods, indicating that the Fe(III) ion accepts more electron density than the Mn(II) ion. This tendency is consistent with our previous study on manganese complexes.[40] These results indicate that the Fe−O bond is stronger than the Mn−O bond, leading to the shorter Fe−O bond.

Since the spin density on the bridging ligand of **1** was almost zero, it is obvious that the spin delocalization on the Fe−O site is weak. The cap hydrogen of the μ-hydroxo ligand weakens the spin delocalization from the bridging ligand. The spin density on the bridging ligand of **2** indicates the α spin delocalization from the Fe ion, causing the direct spin coupling between the bridging oxygen site and the Mn(II) ion. This is responsible for the strong antiferromagnetism of **2**.

3.3. Natural Orbital Analysis. Singly occupied natural orbitals (SONOs), determined by the UB3LYP calculations of **1** and **2**, are depicted in Figures 4 and 5, respectively. In Figure 4, SONO-5 and SONO+5 show the σ-type interactions via the bridging μ-hydroxo ligand. SONO-4, SONO-3, SONO+3, and SONO+4 indicate the π-type interactions via the bridging ligand. SONO-2, SONO-1, SONO+1, and SONO+2 have the δ-type interactions via the μ-hydroxo ligand. As shown in Figure 4, the bonding and antibonding SONOs of **1** are symmetric and delocalized over the binuclear metal core, indicating the superexchange system, consistent with the previous studies of the μ-oxo- and μ-hydroxo-bridged manganese porphyrin and hemerythrin.[14,19,20]

As shown in Figure 5, the shapes of the bonding and antibonding SONOs of **2** are asymmetric. The Fe−O parts of SONO±5, SONO±4, and SONO±3 exhibit an antibonding nature, indicating the β spin delocalization from the μ-oxo ligand to Fe(III) and the strong bonding character of the Fe−O bond, as illustrated in Figure 6.There are three doubly occupied natural orbitals (σ, π1, and π2), which indicate the Fe−O bond. Since the bonding orbital of the Fe−O bond is fully occupied, the singly occupied antibonding MO interacts with the 3d orbital of Mn(II), contributing to the stabilization of **2**. SONO-5 shows the σ-type interaction between the π*-type MO of the Fe−O part and the 3d orbital of the Mn(II) ion. SONO-4 has the π-type interaction between the π*-type MO of the Fe−O part and the 3d orbital of the Mn(II) ion. SONO-3 is the π-type interaction between the σ*-type MO of the Fe−O part and the 3d orbital of the Mn(II) ion. The direct exchange interaction caused by the orbital interactions between the Fe−O part and the Mn ion is the origin of the stronger antiferromagnetism of **2** than **1**.

3.4. Chemical Indices. Chemical indices are useful to investigate the nature of a chemical bond. To analyze the magnetic interaction from the viewpoint of chemical bonds, we introduced the effective bond order and the diradical character. Table 4 lists the effective bond order, b_i, and the diradical character, Y_i, of the SONOs for **1** and **2**.

A comparison of the effective bond orders between **1** and **2** revealed that the active site of **2** shows stronger bonding than that of **1**, because the spin delocalization interaction of **2** is stronger than that of **1**. The strong spin delocalization interaction is the main origin of the larger absolute value of the effective exchange integral of **2**. The effective bond orders show that the order of contribution to antiferromagnetism is $\sigma > \pi \gg \delta$. The diradical characters show the tendency of the chemical bond instability as $\delta \gg \pi > \sigma$. These results suggest that the main pathways of magnetic exchange are σ- and π-type interactions. The effective bond orders and the diradical characters indicate that the σ interaction is rather strong. The effective bond orders of **2** were larger than those of **1**. This tendency indicates that the orbital overlaps of the α and β unrestricted MOs of **2,** which are included in a natural orbital, are larger than those of **1**. These results indicated that the spin delocalization interaction of the Fe−O site strengthens the antiferromagnetism of this system.

4. Conclusion

We have investigated the origin of the stronger antiferromagnetism of the active site of sweet potato PAP, using UHF, pure DFT, and hybrid DFT calculations. The effective exchange

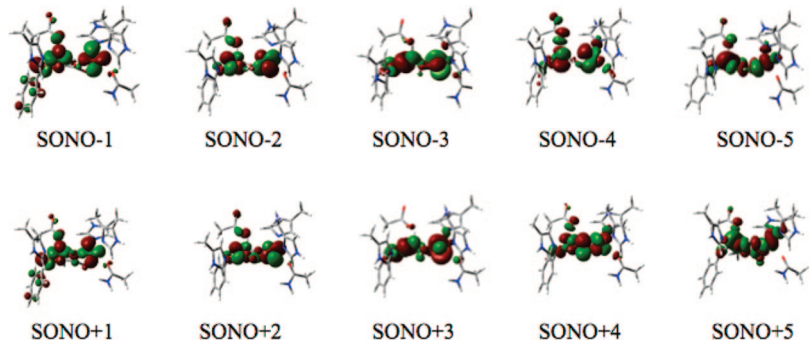

Figure 4. Bonding (SONO-5 to SONO-1) and antibonding (SONO+1 to SONO+5) singly occupied natural orbitals (SONOs) of **1** at the UB3LYP level of theory.

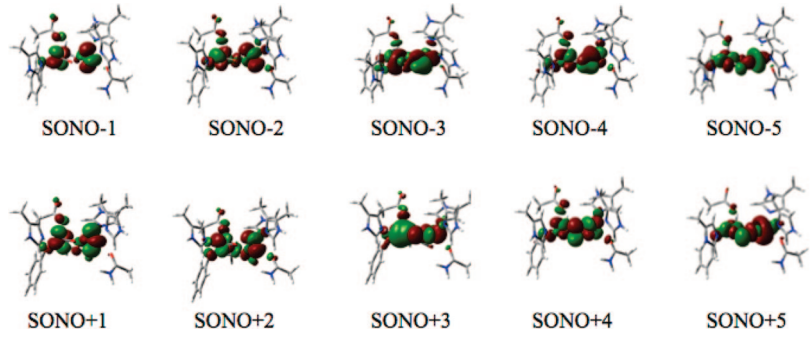

Figure 5. Bonding (SONO-5 to SONO-1) and antibonding (SONO+1 to SONO+5) singly occupied natural orbitals (SONOs) of **2** at the UB3LYP level of theory.

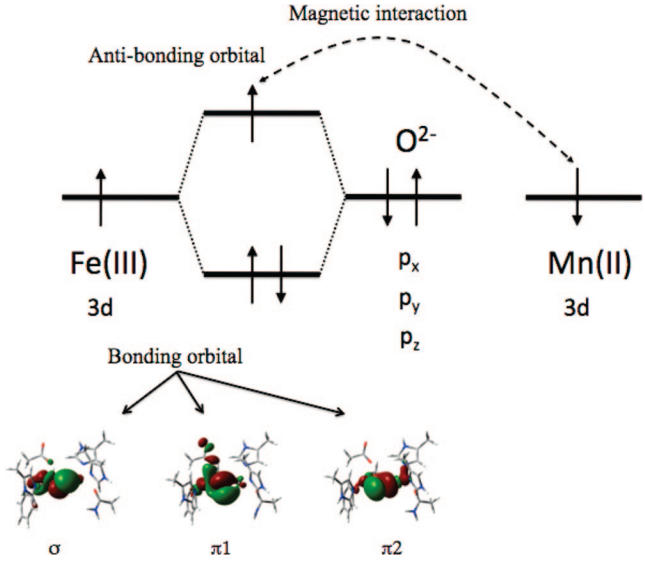

Figure 6. Schematic view of the orbital interactions in the Fe(III)−O^{2-}−Mn(II) core. Doubly occupied natural orbitals, which indicate the bond between Fe and O, are also presented.

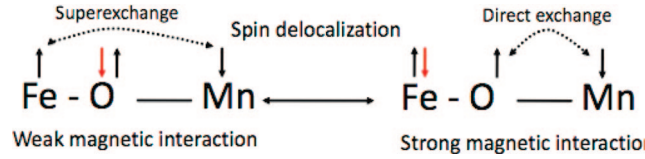

Figure 7. Schematic view of the magnetic interaction in the Fe(III)−O^{2-}−Mn(II) core of the active site of sweet potato PAP. Spin delocalization introduces the character of direct interaction into the asymmetric superexchange interaction. This is the main origin of the stronger antiferromagnetic coupling of the sweet potato PAP active site.

TABLE 4: Effective Bond Order, b_i, and Diradical Character, Y_i, for SONOs of 1 and 2 in the LS State at the UB3LYP Level of Theory[a]

model		SONO-5	SONO-4	SONO-3	SONO-2	SONO-1
1	b_i	0.122	0.072	0.063	0.035	0.019
	Y_i	0.76	0.86	0.87	0.93	0.96
2	b_i	0.236	0.180	0.116	0.036	0.014
	Y_i	0.55	0.65	0.70	0.93	0.97

[a] The positions of the metal ions, the bridging ligand (μ-hydroxo or μ-oxo), and the hydrogen atoms were optimized at the UB3LYP level of theory.

integral calculated by UB3LYP is consistent with the experimental results and strongly supports the μ-oxo bridging ligand in the binuclear metal center. This result is useful for further studies, such as investigations of reaction mechanisms. The atomic charge and spin density distributions of **2** indicate the spin delocalization on the Fe−O, caused by the intrinsic nature of Fe(III), which accepts more electron density than Mn(II). The shapes of the natural orbitals of **2** reflect the bonding nature of the Fe−O site. The main pathways of antiferromagnetic coupling are the σ- and π-type interactions. The spin delocalization on the Fe−O site adds the direct exchange interaction to the superexchange interaction, resulting in the strong antiferromagnetic coupling as shown in Figure 7. These results are consistent with the analysis of chemical indices, calculated by using the occupation numbers of natural orbitals.

Acknowledgment. This work was supported by grants from the New Energy and Industrial Technology Development Organization of Japan (NEDO) and the Ministry of Economy, Trade, and Industry (METI) of Japan. We are grateful to the Ministry of Education, Culture, Sports, Science and Technology (MEXT) Japan for Grants-in Aid for Scientific Research on Priority Areas "Structures of Biological Macromolecular Assemblies" (513-18054013 and 513-20051013) and the Grant-in Aid for Encouragement of Young Scientists (18750011). We

also thank the Japan Society for the Promotion of Science for the Grant-in-Aid for Scientific Research (B) (18370063). The computations were performed at the Research Center for Computational Science, Okazaki, Japan and the Cybermedia Center at Osaka University, Japan.

Supporting Information Available: Occupation numbers of natural orbitals (Table S1), Mulliken atomic spin and charge densities, effective bond orders, and diradical characters estimated by UHF, UB2LYP, and UBLYP (Tables S2 and S3), total energies and $\langle S^2 \rangle$ values used for the deduction of effective exchange integrals (Table S4), and ligand−metal distances of **1** and **2** (Figures S1 and S2). This material is available free of charge via the Internet at http://pubs.acs.org.

References and Notes

(1) Lindqvist, Y.; Johansson, E.; Kaija, H.; Vihko, P.; Schneider, G. *J. Mol. Biol.* **1999**, *291*, 135.

(2) Guddat, L. W.; McAlpine, A. S.; Hume, D.; Hamilton, S.; de Jarsey, J.; Martin, J. L. *Structure* **1999**, *7*, 757.

(3) Strater, N.; Jasper, B.; Scholte, M.; Krabs, B.; Duff, A. P.; Langley, D. B.; Han, R.; Averill, B. A.; Freeman, H. C.; Guss, J. M. *J. Mol. Biol.* **2005**, *351*, 233.

(4) Klabunde, T.; Strater, N.; Frohich, R.; Witzel, H.; Krebs, B. *J. Mol. Biol.* **1996**, *259*, 737.

(5) Schenk, G.; Gahan, L. R.; Carrington, L. E.; Mitic, N.; Valizadeh, M.; Hamilton, S. E.; de Jersey, J.; Guddat, L. W *Proc. Natl. Acad. Sci. U.S.A.* **2005**, *102*, 273.

(6) Schenk, G.; Boutchard, C. L.; Carrington, L. E.; Noble, C. J.; Moubaraki, B.; Murray, K. S. *J. Biol. Chem.* **2001**, *276*, 19084.

(7) Wilcox, D. E. *Chem. Rev.* **1996**, *96*, 2435.

(8) Maruno, Y.; Shoji, M.; Koizumi, K.; Nishiyama, Y.; Kitagawa, Y.; Kawakami, T.; Okumura, M.; Yamaguchi, K. *Polyhedron* **2005**, *24*, 2778.

(9) Smoukov, S. K.; Quaroni, L.; Wang, X.; Doan, P. E.; Hoffman, B. M.; Que, L. *J. Am. Chem. Soc.* **2002**, *124*, 2595.

(10) Averill, B. A.; Davis, J. C.; Burman, S. J.; Sanders-Loehr, J.; Loeher, T. M.; Sage, T. J.; Debrunner, P. G. *J. Am. Chem. Soc.* **1987**, *109*, 3760.

(11) Antanaitis, B. C.; Aisen, P.; Lilienthal, H. R. *J. Biol. Chem.* **1983**, *258*, 3166.

(12) Lauffer, R. B.; Antanaitis, B. C.; Aisen, P.; Que, L., Jr. *J. Biol. Chem.* **1983**, *258*, 14212.

(13) Day, E. P.; David, S. S.; Peterson, J.; Dunham, W. R.; Bonvoisin, J. J.; Sands, R. H.; Que, L., Jr. *J. Biol. Chem.* **1988**, *263*, 15561.

(14) Koizumi, K.; Shoji, M.; Kitagawa, Y.; Ohoyama, H.; Kasai, T.; Yamaguchi, K. *Eur. Phys. J. D* **2006**, *38*, 193.

(15) Shoji, M.; Isobe, H.; Takano, Y.; Kitagawa, Y.; Yamanaka, S.; Okumura, Y.; Yamaguchi, K. *Int. J. Quantum Chem.* **2007**, *107*, 3250.

(16) (a) Siegbahn, P. E. M.; Crabtree, R. H. *J. Am. Chem. Soc.* **1997**, *119*, 3113. (b) Siegbahn, P. E. M *Inorg. Chem.* **1999**, *38*, 2880. (c) Siegbahn, P. E. M. *Chem. Phys. Lett.* **2002**, *351*, 311.

(17) Yoon, Y.; Liboiron, B. D.; Sarangi, R.; Hodgson, K. O.; Hedman, B.; Solomon, E. I. *Proc. Natl. Acad. Sci. U.S.A.* **2007**, *104*, 13609.

(18) Noodleman, L.; Peng, C. Y.; Case, D. A.; Mouesca, J.-M. *Coord. Chem. Rev.* **1995**, *144*, 199.

(19) Shoji, M.; Hamamoto, T.; Koizumi, K.; Isobe, H.; Kitagawa, Y.; Takano, Y.; Yamanaka, S.; Yamaguchi, K. *Polyhedron* **2005**, *24*, 2701.

(20) Takano, Y.; Isobe, H.; Yamaguchi, K. *Bull. Chem. Soc. Jpn.* **2008**, *81*, 91.

(21) Itoh, K.; Kinoshita, M., Eds. *Molecular Magnetism: New Magnetic Materials*; Kodansha-Godon and Breach: Tokyo, Japan, 2000.

(22) Kahn, O., Ed. *Magnetism: A Supramolecular Function*; NATO ASI Series C; Kluwer Academic Publishers: Dordrecht, The Netherlands, 1996; Vol. 484.

(23) Yamaguchi, K.; Takahara, Y.; Fueno, T. In *Applied Quantum Chemistry*; Smith, V. H., Schaefer, H. F., III., Morokuma, K., Eds.; Reidal: Boston, MA, 1986.

(24) Parr, R. G.; Young, W. *Density Functional Theory of Atoms and Molecules*; Oxford University Press: Oxford, UK, 1989.

(25) Trickey, S. B., Ed. *Density Functional Theory of Many Fermion Systems*; Advances in Quantum Chemistry, Vol. 21; Academic Press: San Diego, CA, 1990.

(26) Becke, A. D. *Phys. Rev. A* **1988**, *38*, 3098.

(27) Vosko, S. H.; Wilk, L.; Nusair, M. *Can. J. Phys* **1980**, *58*, 785.

(28) Lee, C.; Yang, W.; Parr, R. G. *Phys. Rev. B* **1988**, *37*, 785.

(29) Becke, A. D. *J. Chem. Phys.* **1993**, *98*, 5648.

(30) (a) Takano, Y.; Kitagawa, Y.; Onishi, T.; Yoshioka, Y.; Yamaguchi, K.; Koga, N.; Iwamura, H. *J. Am. Chem. Soc.* **2002**, *124*, 450. (b) Takano, Y.; Soda, T.; Kitagawa, Y.; Yoshioka, Y.; Yamaguchi, K. *Chem. Phys. Lett.* **1999**, *301*, 309. (c) Takano, Y.; Soda, T.; Kitagawa, Y.; Onishi, T.; Yoshioka, Y.; Yamaguchi, K. *Int. J. Quantum Chem.* **2000**, *80*, 681.

(31) Isobe, H.; Takano, Y.; Kitagawa, Y.; Kawakami, T.; Yamanaka, S.; Yamaguchi, K.; Houk, K. N. *Mol. Phys.* **2002**, *100*, 717.

(32) Mitani, M.; Yamaki, D.; Takano, Y.; Kitagawa, Y.; Yoshioka, Y.; Yamaguchi, K. *J. Chem. Phys.* **2000**, *113*, 10486.

(33) Tatewaki, H.; Huzinaga, S. *J. Chem. Phys.* **1980**, *72*, 339.

(34) Hariharan, P. J.; Pople, J. A. *Theor. Chem. Acta* **1973**, *28*, 213.

(35) Hehre, W. J.; Ditchfild, R.; Pople, J. A. *J. Chem. Phys.* **1972**, *56*, 2257.

(36) Frisch, M. J.; Trucks, G. W.; Schlegel, H. B.; Scuseria, G. E.; Robb, M. A.; Cheeseman, J. R. , Montgomery, J. A., Jr.; Vreven, T.; Kudin, K. N.; Burant, J. C.; Millam, J. M.; Iyenger, S. S.; Tomasi, J.; Barone, V.; Mennucci, B.; Cossi, M.; Scalmani, G.; Rega, N.; Petersson, G. A.; Nakatsuji, H.; Hada, M.; Ehara, M.; Toyota, K.; Fukuda, R.; Hasegawa, J.; Ishida, M.; Nakajima, T.; Honda, Y.; Kitao, O.; Nakai, H.; Klene, M.; Li, X.; Knox, J. E.; Hratchian, H. P.; Cross, J. B.; Bakken, V.; Adamo, C.; Jaramillo, J.; Gomperts, R.; Startmann, R. E.; Yazyev, O.; Austin, A. J.; Cammi, R.; Pomelli, C.; Ochterski, J. W.; Ayala, P. Y.; Morokuma, K.; Voth, G. A.; Salvador, P.; Dannenberg, J. J.; Zakrzewski, V. G.; Dapprich, S.; Daniels, A. D.; Strain, M. C.; Farkas, O.; Malick, D. K.; Rabuck, A. D.; Raghavachari, K.; Foresman, J. B.; Ortiz, J. V.; Cui, Q.; Baboul, A. G.; Clifford, S.; Cioslowski, J.; Stefanov, B. B.; Liu, G.; Liashenko, A.; Piskorz, P.; Komaromi, I.; Martin, R. L.; Fox, D. J.; Keith, T.; Al-Laham, M. A.; Peng, C. Y.; Nanayakkara, A.; Challacombe, M.; Gill, P. M. W.; Johnson, B.; Chen, W.; Wong, M. W.; Gonzalez, C.; Pople, J. A. *Gaussian 03*, Revision C.02; Gaussian, Inc., Wallingford, CT, 2004.

(37) Brunold, T. C.; Solomon, E. I. *J. Am. Chem. Soc.* **1999**, *121*, 8277.

(38) Kitagawa, Y.; Saito, T.; Ito, M.; Shoji, M.; Koizumi, K.; Yamanaka, S.; Kawakami, T.; Okumura, M.; Yamaguchi, K. *Chem. Phys. Lett.* **2007**, *442*, 445.

(39) Wirstam, M.; Lippard, S. J.; Friesner, R. A. *J. Am. Chem. Soc.* **2003**, *125*, 3987.

(40) Koizumi, K.; Shoji, M.; Nishiyama, Y.; Maruno, Y.; Kitagawa, Y.; Soda, K.; Yamanaka, S.; Okumura, M.; Yamaguchi, K. *Int. J. Quantum Chem.* **2004**, *100*, 943.

JP8090123